Biochemistry

pubs.acs.org/biochemistry Article

Atomic-Resolution 1.3 Å Crystal Structure, Inhibition by Sulfate, and Molecular Dynamics of the Bacterial Enzyme DapE

Matthew Kochert, Boguslaw P. Nocek, Thahani S. Habeeb Mohammad, Elliot Gild, Kaitlyn Lovato, Tahirah K. Heath, Richard C. Holz, Kenneth W. Olsen,* and Daniel P. Becker*

Cite This: *Biochemistry* 2021, 60, 908–917 Read Online

ACCESS | Metrics & More | Article Recommendations | Supporting Information

ABSTRACT: We report the atomic-resolution (1.3 Å) X-ray crystal structure of an open conformation of the *dapE*-encoded *N*-succinyl-L,L-diaminopimelic acid desuccinylase (DapE, EC 3.5.1.18) from *Neisseria meningitidis*. This structure [Protein Data Bank (PDB) entry 5UEJ] contains two bound sulfate ions in the active site that mimic the binding of the terminal carboxylates of the *N*-succinyl-L,L-diaminopimelic acid (L,L-SDAP) substrate. We demonstrated inhibition of DapE by sulfate (IC_{50} = 13.8 ± 2.8 mM). Comparison with other DapE structures in the PDB demonstrates the flexibility of the interdomain connections of this protein. This high-resolution structure was then utilized as the starting point for targeted molecular dynamics experiments revealing the conformational change from the open form to the closed form that occurs when DapE binds L,L-SDAP and cleaves the amide bond. These simulations demonstrated closure from the open to the closed conformation, the change in RMS throughout the closure, and the independence in the movement of the two DapE subunits. This conformational change occurred in two phases with the catalytic domains moving toward the dimerization domains first, followed by a rotation of catalytic domains relative to the dimerization domains. Although there were no targeting forces, the substrate moved closer to the active site and bound more tightly during the closure event.

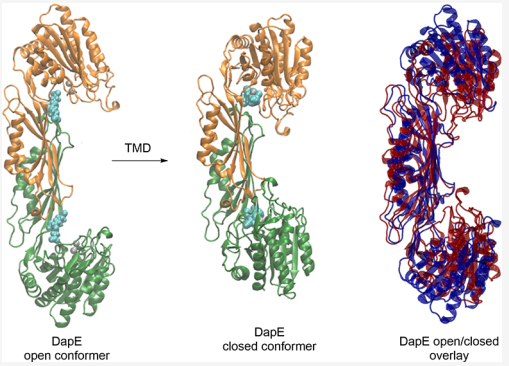

The rapid rise in morbidity and mortality from bacterial infections caused by antibiotic-resistant bacteria[1] underlines the need to discover antibiotics with a new mechanism of action by targeting previously unexplored bacterial enzymes. For example, invasive methicillin-resistant *Staphylococcus aureus* (MRSA) is a serious and growing health problem.[2] Several newly discovered strains of MRSA show antibiotic resistance even to vancomycin, which is considered a last resort for the treatment of systemic infections.[3] An attractive but underexplored bacterial target that is present in all Gram-negative and most Gram-positive bacteria is the *dapE*-encoded *N*-succinyl-L,L-diaminopimelic acid desuccinylase (DapE, EC 3.5.1.18).[4] DapE is a member of the lysine biosynthetic pathway in bacteria that is responsible for the synthesis of lysine and *meso*-diaminopimelate (*m*-DAP),[5] both of which are critical for peptidoglycan cell-wall synthesis. DapE enzymes catalyze the hydrolysis of *N*-succinyl-L,L-diaminopimelic acid (L,L-SDAP) to succinate and L,L-diaminopimelic acid [L,L-DAP (Figure 1)].

Deletion of the *dapE* gene is lethal to *Helicobacter pylori* and *Mycobacterium smegmatis*, demonstrating the indispensable role of this enzyme in bacterial survival, and therefore pathogenesis in the human host.[7,8] Furthermore, the lack of a similar pathway in humans suggests that inhibition of DapE should be selectively toxic to bacteria but not human hosts, making it a promising target for antibiotics with a new mechanism of action free of mechanism-based side effects.[4] To conveniently measure the inhibitory potency of test compounds versus DapE, we previously reported a ninhydrin-based assay[6] employing the substrate N^6-methyl-L,L-SDAP (**1b**), which when cleaved by DapE affords primary amine product **3b** (Figure 1) that can be quantified spectrophotometrically after treatment with ninhydrin.

The first X-ray crystal structure of an apo DapE from *Neisseria meningitidis* (*Nm*DapE) was determined in 2005[9] and was followed by structures of mono- and di-Zn forms from *Haemophilus influenzae* (*Hi*DapE)[10] and mono- and di-Zn forms from *Nm*DapE.[11] Significantly, the structure of the DapE inhibitor captopril bound to the active site demonstrated interactions of the thiol moiety with the active site zinc atoms.[11] We recently reported a DapE crystal structure revealing the previously unknown closed conformation of dimeric DapE with the products of enzymatic cleavage, succinate and diaminopimelic acid, bound in the active site

Received: November 25, 2020
Revised: March 8, 2021
Published: March 16, 2021

https://dx.doi.org/10.1021/acs.biochem.0c00926
Biochemistry 2021, 60, 908–917

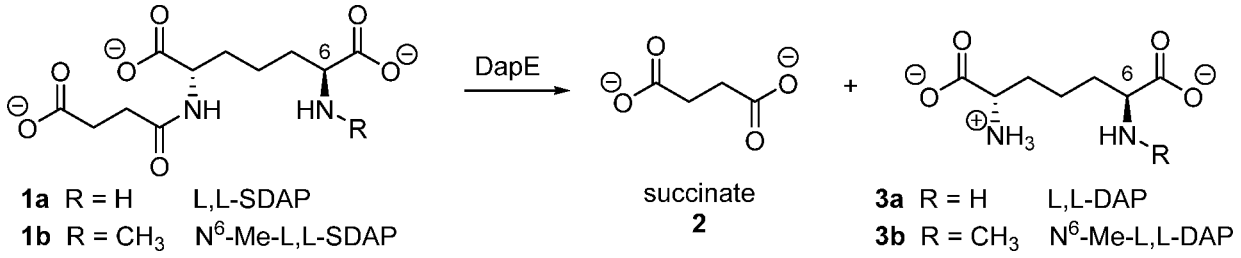

Figure 1. Hydrolysis of L,L-SDAP by DapE. L,L-SDAP (**1a**) and assay substrate N^6-methyl-L,L-SDAP[6] (**1b**) with formation of hydrolysis products succinate (**2**) and L,L-diaminopimelic acid derivatives **3a** and **3b**, respectively.

[Protein Data Bank (PDB) entry 5VO3].[12] This structure also revealed the role of His195B, a residue on the opposite subunit that moves ∼10 Å and provides a key H-bond to the substrate in the active site.[12] The requirement of this His residue explains the observed inactivity of a truncated, monomeric construct of DapE.[6] The product-bound structure, aided by our product-bound transition state modeling (PBTSM) approach,[12,13] enabled further refinement of the proposed reaction mechanism of DapE that will facilitate inhibitor identification[14−16] for the discovery of new antibiotics that inhibit DapE.

We report herein a new atomic-resolution (1.3 Å) X-ray crystal structure of *Nm*DapE (PDB entry 5UEJ) with sulfate ions bound in the substrate recognition pocket. Our previous closed product-bound structure of *Hi*DapE[12] in combination with this new high-resolution open structure further defines the dramatic conformational range of motion that occurs for DapE during its catalytic cycle and enabled us to explore this remarkable conformational process using targeted molecular dynamics (TMD).

EXPERIMENTAL SECTION

Protein Preparation and Crystallization. *Nm*DapE was expressed in *Escherichia coli* and prepared according to a protocol described previously.[6,11,12] Bacteria were cultured while being shaken at 210 rpm in LB medium supplemented with 150 μg/mL ampicillin at 37 °C until the OD_{600} reached 1.0. The temperature was decreased to 18 °C, and isopropyl D-thiogalactopyranoside (IPTG) was added to a final concentration of 0.5 mM. The culture was grown for 18 h and then centrifuged at 4500 rpm for 10 min at 4 °C. The cell pellet derived from 1 L of culture was resuspended in 35 mL of lysis buffer [50 mM HEPES sodium salt (pH 8.0), 500 mM NaCl, 5% glycerol, 20 mM imidazole, and 10 mM β-mercaptoethanol] and stored at −80 °C. The samples were thawed, and the cells were disrupted by sonication using bursts totaling 5 min in duration, with appropriate intervals for cooling. The cell debris was then pelleted by centrifugation at 15000 rpm for 30 min at 4 °C. The supernatant was applied to a column packed with 10 mL of HisTrap HP resin (GE Healthcare), connected to a VacMan (Promega), and the chromatographic process was accelerated with a vacuum pump. The column was washed with 20 bed volumes of lysis buffer, and the His_6-tagged P5CRs were eluted with 25 mL of elution buffer [50 mM HEPES (pH 8.0), 500 mM NaCl, 500 mM imidazole, and 2 mM DTT]. The His_6 tag was cleaved with TEV protease (2 mg of a His_6-tagged form) overnight at 4 °C, and dialysis to remove the excess imidazole was carried out simultaneously. The resulting solution was mixed with His-Trap HP resin to capture the cleaved His_6 tag and the His_6-tagged TEV protease with the flow-through containing the DapE protein, which was collected and concentrated. The next step required running the sample through a HiLoad 16/600 Superdex 200 Prep grade column and eluting with the crystallization buffer.

Crystal Structure of *Nm*DapE at 1.3 Å Resolution. Crystals were grown using freshly purified protein (∼20 mg/mL) by the sitting drop method at 17 °C employing a precipitant solution of 0.2 M Li_2SO_4, 0.1 M Tris (pH 8.5), 1.26 M $(NH_4)_2SO_4$, and 0.05 M DMSO over several weeks. The crystals belonged to the $P2_12_12_1$ space group with unit cell parameters of a = 74.8 Å, b = 88.6 Å, c = 133.4 Å, and $\alpha = \beta = \gamma = 90°$ with a single dimer in the asymmetric unit (Table S1), consistent with *Nm*DapE in solution, which is a dimer. Prior to data collection, the mother liquor containing 25% glycerol was used as a cryoprotectant. A single crystal was picked up with a MiTeGen loop and flash-frozen in liquid nitrogen. The data set was collected at the 19-ID[17] beamline of the Structural Biology Center at the Advanced Photon Source, Argonne National Laboratory. All data sets were processed using the HKL3000[18] suite of programs. Data collection statistics are listed in Table S1. The high-resolution crystal structure of DapE was determined using the molecular replacement method employing MolRep[19] using the previously determined structure of *Nm*DapE. Cycles of manual corrections of the model were carried out in COOT,[20] and the refinement routine was implemented in Refmac.fva.[21] The crystals diffracted to near atomic resolution, 1.30 Å, compared to the best resolution previously obtained for a DapE structure of 1.80 Å. This improvement in resolution allowed us to refine the structure anisotropically and to determine more detailed and accurate positions of atoms, reliable recognition of alternative conformations, and the correct positions of hydrogen atoms. This in turn enables more accurate docking and molecular dynamics studies that will ultimately enhance inhibitor design. The model of the structure has R_{work} and R_{free} values of 11% and 15%, respectively. The structure was analyzed and validated with the aid of MOLPROBITY and COOT validation tools.[22,23] Figures were prepared using VMD.[24] The atomic coordinates and the structure factor file for this new open form of *Nm*DapE have been deposited in the RCSB Protein Bank as entry 5UEJ.

Enzyme Assays. *Inhibition of DapE by Sulfate: IC_{50} Determination.* The inhibition of *Hi*DapE by sulfate was assessed using lithium sulfate following the protocol detailed by us previously[6] with slight modifications as detailed below. All inhibition assays were conducted with a reaction volume of 200 μL, 2 mM N^6-methyl-L,L-SDAP, and 8 nM *Hi*DapE. To a 50 mM HEPES (pH 7.5) buffered solution at 30 °C was added lithium sulfate followed by *Hi*DapE, and the mixture was incubated for 10 min at 30 °C. N^6-Methyl-L,L-SDAP was added and allowed to react for 10 min at 30 °C, and then the mixture was heated to 100 °C for 1 min and cooled on ice to 0 °C. A

https://dx.doi.org/10.1021/acs.biochem.0c00926
Biochemistry 2021, 60, 908−917

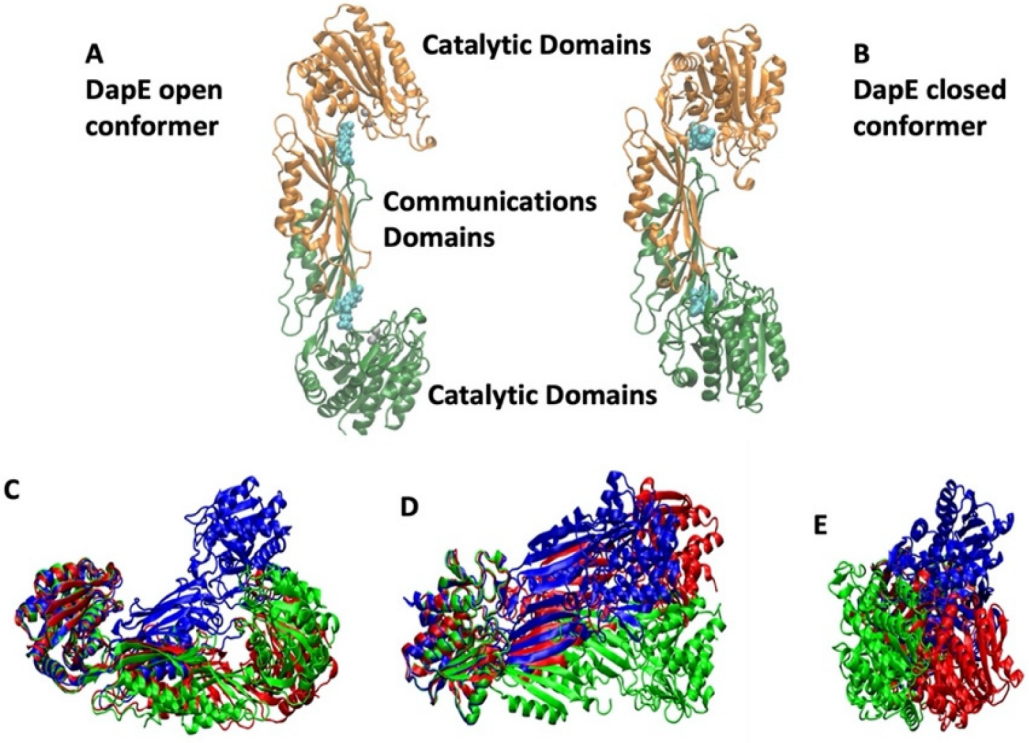

Figure 2. DapE enzyme X-ray crystal structures illustrating conformational changes. (A) DapE open conformation of *Nm*DapE (PDB entry 5UEJ) with the substrate shown in blue space-filling atoms modeled in the active site. (B) Closed conformation of *Hi*DapE (PDB entry 5VO3) with the bound substrate modeled in space-filling blue atoms. (C–E) Overlap of three different DapE structures: the new high-resolution open *Nm*DapE structure (PDB entry 5UEJ, red), the 2.30 Å resolution open *Hi*DapE structure (PDB entry 3IC1, green), and the product-bound *Nm*DapE structure (PDB entry 5VO3, blue). The A chains for all three proteins are superimposed on the left side of panels C–E showing the different positions of the B chains on the right side of each representation, with each panel showing mutually perpendicular views of the three overlapped structures.

2% ninhydrin solution (100 μL) was added, and the mixture was vortexed. The reaction mixture was heated to 80 °C for 15 min followed by cooling on ice. The absorbance of an 80 μL aliquot was recorded at 570 nm on a BioTek Synergy 2 microplate reader. The inhibition of *Hi*DapE by lithium sulfate was assayed in triplicate, and the IC_{50} was determined to be 13.8 ± 2.8 mM. The IC_{50} and kinetic constants were obtained by fitting the data to the modified Hill equation $V = V_0 + (V_{max} - V_0)X^{n_H}/(X^{n_H}{}_{0.5} + X^{n_H})$ using the graphing suite Origin 9.1 with the Levenberg–Marquardt nonlinear least-squares algorithm.[25,26] The velocity in the absence of the substrate is V_0. The velocity at saturating concentrations of the substrate or with no inhibitor for the inhibition assay is V_{max}. The concentration of the substrate or inhibitor is X. $X_{0.5}$ is the substrate ($S_{0.5}$) and inhibitor ($I_{0.5}$) concentration at 50% maximum velocity and 50% inhibition, respectively. The Hill coefficient is represented as n_H. The inhibition plots are shown in Figure S3-S8.

Kinetic Studies. A discontinuous kinetic assay was performed on a Techne PCR Thermal Cycler System utilizing a modified ninhydrin assay protocol[6] as mentioned above. All of the experiments were performed in 50 mM HEPES buffer at pH 7.5. The volume of each component was adjusted to fit the total reaction volume of 50 μL, and the enzyme concentration was 0.12 μM. Inhibition of *Hi*DapE with 10, 20, and 30 mM lithium sulfate was studied in triplicate while the substrate concentration was increased from 0.5 to 5.5 mM. The amount of *N*-methyl-L,L-DAP formed over 10 min at 30 °C was monitored by measuring the absorbance of the complex formed by reacting *N*-methyl-L,L-DAP with 2% ninhydrin. The enzymatic activity was reported as the rate of formation of the product, *N*-methyl-L,L-DAP, in absorbance units per minute (AU/min). The kinetic constants were reproducible within ±11% using the modified Hill equation utilizing the Levenberg–Marquardt nonlinear least-squares algorithm.[25]

Sequence Comparisons. The nonrepetitive sequence database was searched for homologues of *Nm*DapE using the blastp algorithm.[27] The sequences for the 99 DapE proteins found were aligned using the Clustal Omega algorithm.[28]

Targeted Molecular Dynamics. The starting structure for TMD experiments was the new PDB entry 5UEJ structure. The target structure used for these simulations was a homology model of the closed structure (PDB entry 5VO3) that had the sequence of the open structure (PDB entry 5UEJ) and was created using SwissModel.[29] The two sequences were 55.1% identical, which is sufficient to produce a good homology model.[30] The structural assessment of the model using the tools available through Swiss-Model showed that it was a high-quality model. For molecular dynamics experiments, each simulation box containing either the open or the closed conformation of DapE, the substrate, and the catalytic zinc ions was assembled using the molecular graphics program VMD.[24] The simulation box was then brought to equilibrium using the molecular dynamics program NAMD.[31] The equilibration procedure involved energy minimization with and without restraints on the protein coordinates (3000 steps each), slow heating from 10 to 310 K (60 ps), and then pressure and temperature equilibration using a Langevin piston

https://dx.doi.org/10.1021/acs.biochem.0c00926
Biochemistry 2021, 60, 908–917

(20 ps). Finally, unrestrained dynamics for 2 ns was performed before data were acquired. Periodic boundary conditions were used. The cutoffs for nonbonding (van der Waals and electrostatic) interactions were 15 Å. The switch distance was 13 Å, and a 1.0 1−4 scaling factor was used. In the TMD simulations, the force constant set for the calculations was 1000 kcal mol^{-1} $Å^{-2}$. The simulation was run for a total of 50 ns. The time step was 1 fs, and every 500th step in the trajectory was saved for analysis. All calculations were performed using CHARMM 36 parameters.[32−35] The zinc ion in this force field is represented by electrostatic and van der Waals potentials. The total interaction energy values were determined every 0.1 ns in each set of simulations. All molecular graphics diagrams were generated using VMD.[24] The sulfur atom coordinates from the sulfates in the crystal structure were used to assign the coordinates of the carboxylate carbon atoms found at both ends of the substrate. The rest of the substrate atoms were then built, and the energy of the overall structure was minimized. In the closed structure, the product positions were used as a reference for where the substrate should be built. Once the substrate was constructed, a water box with 0.15 M NaCl was built enclosing both DapE and the substrate to neutralize charges and mimic a physiological environment for the enzyme and substrate. The structure was then equilibrated for 2 ns to allow each system to achieve a local minimum energy conformation. TMD simulations were then run for 50 ns using this equilibrated structure. The equilibrated structure was then re-equilibrated twice for an additional 2 ns each. The TMD simulations were then re-run twice for 50 ns using these re-equilibrated structures. The target structure used for these simulations was a homology model of the closed structure (PDB entry 5VO3) that had the sequence of the open structure (PDB entry 5UEJ), which was created using SwissModel.[29]

RESULTS AND DISCUSSION

High-Resolution X-ray Crystal Structure: Comparison and Flexibility of DapE Structures. As expected, the new high-resolution X-ray structure of *Nm*DapE (PDB entry 5UEJ) shares many of the aspects of previously reported *Hi*DapE structures. *Hi*DapE and *Nm*DapE share a high degree of sequence homology of 55% with no sequence gaps and have the same active site architectures, including metal binding residues and substrate binding residues necessary for hydrolytic activity.[14] Both are dimers with two domains in each chain (Figure 2A). The catalytic domain is globular and contains two Zn^{2+} ions and most of the catalytic residues. The catalytic domain in the new *Nm*DapE open structure interacts with the communication domain of the other subunit, but the communication domains from the two chains form most of the intersubunit contacts. There is a significant conformational change observed between the open and closed forms of the enzyme, which likely occurs upon substrate binding (Figure 2A,B).

Comparison of three different DapE crystal structures (PDB entries 5UEJ, 5VO3, and 3IC1) reveals significant differences in the orientations of the domains (Figure 2C−E). The dramatic change from the open to the closed conformation has been noted previously;[12,36] however, even the differences in conformations of available open structures (PDB entries 3IC1 and 5UEJ) are striking, and comparison of eight different DapE structures (Figure S2) underscores the wide range of conformational flexibility of the DapE subunits. The product-bound structure manifests a twist (Figure 2C) different from that of the structures without product, and we have analyzed this change using conformationally sensitive dihedral angles (Figures S1 and S2). Conformational differences may also be due in part to differences in the crystallization conditions (Table S2), and there are many examples of different domain or subunit contacts being found for the same protein due to different crystallization conditions. For example, more than 30 years ago Schiffer and co-workers[37] found that the domains of a Bence-Jones protein could adopt different domain associations depending on the crystallization conditions. For the Bence-Jones structures, the structural changes are limited to the way in which the domains are associated rather than to the folding of the domains themselves, and this is also true for the DapE structures. This ability to adopt different domain arrangements is due to the domains being connected by only one polypeptide strand in the case of Bence-Jones protein or two strands of a polypeptide chain in the case of DapE, allowing flexibility between domains.

Hingelike motions caused by different crystal environments have been seen in many other proteins,[38,39] along with the ability of crystal packing contacts to cause these variations.[40,41] On the contrary, there are even more examples of different domain or subunit arrangements that occur due to the binding of a ligand.[42] The conformational change due to binding of the products by DapE (PDB entry 5VO3 in Figure 2B) is different than the range of flexibility seen for the DapE structures without bound products. A significant twist in the conformation of DapE is demonstrated by changes in selected dihedral angles (Figures S1 and S2) that are notably different for the product-bound structure.

Inhibition of DapE by Sulfate. We observed that two sulfate ions are bound in the new open *Nm*DapE structure (PDB entry 5UEJ) and hypothesized that these sulfates, from the crystallization buffer, occupy the same locations as two of the negatively charged carboxylates of the substrate. This was confirmed by direct comparison of the product-bound *Hi*DapE closed structure (PDB entry 5VO3) with the sulfate-bound *Nm*DapE open structure (PDB entry 5UEJ), where the carboxylates are observed to electrostatically bind to Arg178 and Arg258 of *Hi*DapE, analogous to the sulfates binding Arg179 and Arg259 of *Nm*DapE, respectively (Figure 3). Arginine residues were found in these positions in all of the 99 sequences similar to *Nm*DapE found by a blastp search.

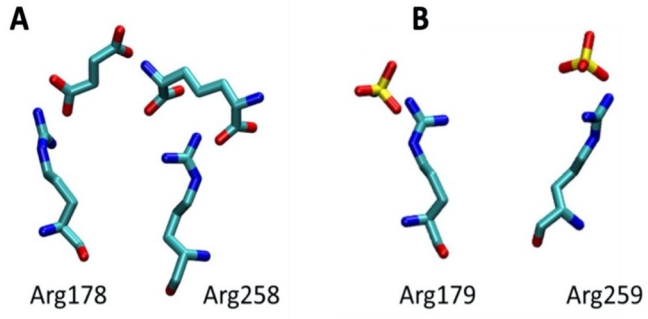

Figure 3. Key Coulombic interactions of (A) the terminal substrate-derived carboxylates of the products in *Hi*DapE (PDB entry 5VO3) with Arg178 and Arg258 and (B) the two bound sulfate ions in the open conformation of *Nm*DapE (PDB entry 5UEJ) with the corresponding arginine residues, Arg179 and Arg259, respectively.

https://dx.doi.org/10.1021/acs.biochem.0c00926
Biochemistry 2021, 60, 908−917

Reviewing all 11 DapE structures deposited in the PDB (summarized in Table S2), we found six of the crystal structures had one or two sulfates bound in their active sites. DapE crystal structures with at least one bound sulfate in the active sites include PDB entries 3IC1 and 3ISZ,[10] as well as PDB entries 4O23, 4PPZ, and 4PQA.[11] The DapE structure that was first reported is an apo structure, PDB entry 1VGY,[9] which lacks bound sulfates, although crystallization conditions were not reported, making it impossible to know if sulfate ions were present in the crystallization solution. Several truncated DapE proteins have been expressed lacking the linker domains and were crystallized in the presence of acetate rather than sulfate (PDB entries 4ONW, 4OP4, and 4H2K)[43] and therefore do not have bound sulfate, but neither do they exhibit bound acetate in their active sites. These truncated DapE proteins are missing the Arg residues that bind the sulfates, or these Arg residues are near the new termini of the protein and thus are in very flexible regions of the structure. Therefore, sulfate binding to these residues would not be expected. Sulfates are well-known to bind at protein phosphate sites,[44,45] and sulfate ions can also compete with carboxylate ions for binding sites.[46]

Realizing that sulfate may compete with the substrate in the active site, we determined the inhibitory potency of sulfate to be 13.8 ± 2.8 mM (IC_{50}) using our ninhydrin-based assay (Figure S3).[6] The concentration of sulfate in the crystallization buffer of PDB entry 5UEJ was 1.46 M, which is 106 times higher than the IC_{50} of sulfate, consistent with its presence in the active site. The only reported product-bound structure (PDB entry 5VO3) did not have sulfate in its crystallization buffer, which was likely more advantageous for substrate binding given the absence of competing sulfate. To investigate the nature of sulfate binding to the DapE active site, we performed a kinetic assay with various substrate and sulfate concentrations. Sulfate inhibition of *Hi*DapE followed a competitive inhibition pattern as summarized in Table 1, and

Table 1. Kinetic Parameters for *Hi*DapE with *N*-Methyl-L,L-SDAP as the Substrate

assay	[sulfate] (mM)	V_{max} (AU/min)	$S_{0.5}$ (mM)
control	0	0.068 ± 0.0055	1.21 ± 0.15
inhibition	10	0.073 ± 0.0072	2.50 ± 0.29
	20	0.080 ± 0.0098	2.72 ± 0.066
	30	0.084 ± 0.0052	2.92 ± 0.098

the saturation curves are reported in Figures S4−S8. The saturation of activity with an increasing substrate concentration was not observed; rather, the enzymatic activity was inconsistent as the pH of the solution started to decline with an increase in *N*-methyl-L,L-SDAP substrate concentration above 5.5 mM. The decrease in the pH of the solution was attributed to the fact that *N*-methyl-L,L-SDAP was synthesized and used as the trifluoroacetate salt of the amine; hence, at higher concentrations, it ultimately affects the pH of the solution.

Targeted Molecular Dynamics. The open conformation DapE structures, including the new high-resolution structure, in comparison with our product-bound closed X-ray crystal structure[12] reveal the dynamic conformational change between the open and closed states of DapE (Figure 4). This conformational change was proposed to be induced by substrate binding, which is consistent with a hinge domain mechanism that enables both domains to interact with the substrate. The *Hi*DapE product-bound structure further revealed several new protein−ligand interactions that had not been predicted by docking or molecular dynamics,[47] including the demonstration of distinct succinate and diaminopimelic acid binding pockets, and that both domains play a key role in substrate recognition and catalysis.

To better understand the catalytically important conformational change of DapE from the open to the closed conformer, TMD simulations were performed. TMD involves application of an additional force on selected atoms in the direction of the positions of their counterparts in the target structure.[48,49] This force depends on the number of atoms selected, the selected force constant, and the root-mean-square deviation (RMSD) between the coordinates at any given time during the simulation and the final coordinates. Three TMD runs were performed from the open to the closed conformation using PDB entry 5UEJ for the open starting DapE conformation and PDB entry 5VO3 for the closed target conformation. The selected atoms were either all of the α-carbons in both subunits or all of the α-carbons in just one of the two subunits. Prior to running TMD simulations, we built the native substrate L,L-SDAP into the active sites of both the initial and target structures, and the system was relaxed as described in the Experimental Section. In the open structure, placement of the substrate was guided by the positions of the two sulfate ions found in the active site of the PDB file to model the positions of the substrate terminal carboxylates. The substrate was placed in the active site of the closed structure in a manner consistent with the binding of the products in PDB entry 5VO3.

The first TMD scenario applied a force to both subunits of DapE in the open conformation. Both subunits approached the closed conformation as measured by their degree of overlap with the target structure (Figure 4A,B). Furthermore, RMSD values comparing the initial structure to the target structure were calculated before and after the simulation to determine the degree of closure. The RMSDs by subunit show nearly complete convergence of the original open structure toward the target closed structure during each run (Figure 4C). The second and third TMD experiments involved applying the additional force only to subunit A and then only to subunit B, respectively. These calculations were performed to investigate if closing one subunit might compel the other subunit to also begin closing. In the simulation with the force applied only to subunit A, that subunit closes as it did with the force applied to both subunits (Figure 5A); however, subunit B does not close or converge toward the target coordinates to any significant extent (Figure 5B). The independence of the two subunits is also supported by the change in RMSD values between the initial structure and the target structure at the beginning and end of the simulation (Figure 5C). In the simulation with the force applied only to subunit B, the simulation plays out in the reverse manner. Subunit B closes completely under these conditions, whereas subunit A does not converge toward the target structure. Changes in the RMSD values between the initial and final structures support this observation that movement was observed only in the subunit to which force was applied (Figure S6A3).

The results of the TMD simulation reported herein can be compared to those of a previous computational study by Dutta and Mishra,[47] who studied the molecular dynamics of apo and L,L-SDAP-bound DapE using principal component analysis

https://dx.doi.org/10.1021/acs.biochem.0c00926
Biochemistry 2021, 60, 908−917

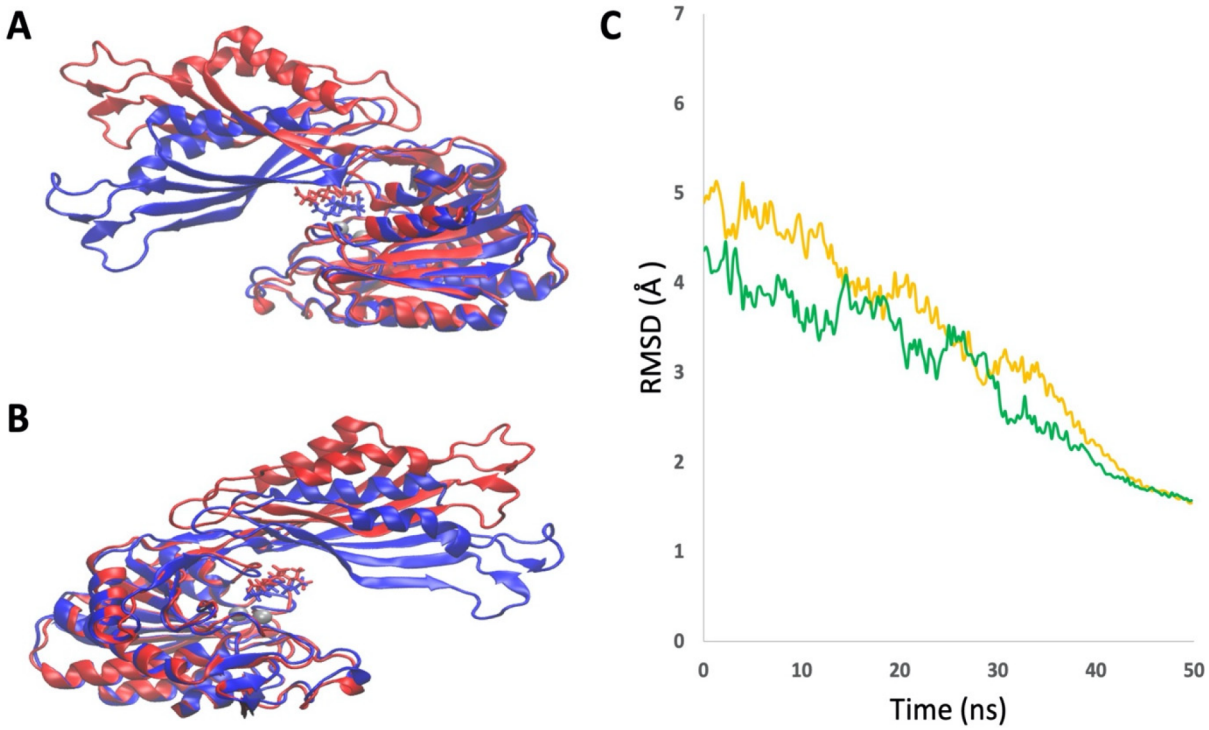

Figure 4. Images of (A) subunit A and (B) subunit B of the DapE enzyme overlaid at 0 (red) and 50 ns (blue) in the simulation with the force on both subunits. The substrate is also shown in both active sites in its position at 0 (red) and 50 ns (blue). (C) Average RMSDs between subunits A (orange) and B (green) in the open structure and their positions in the closed structure.

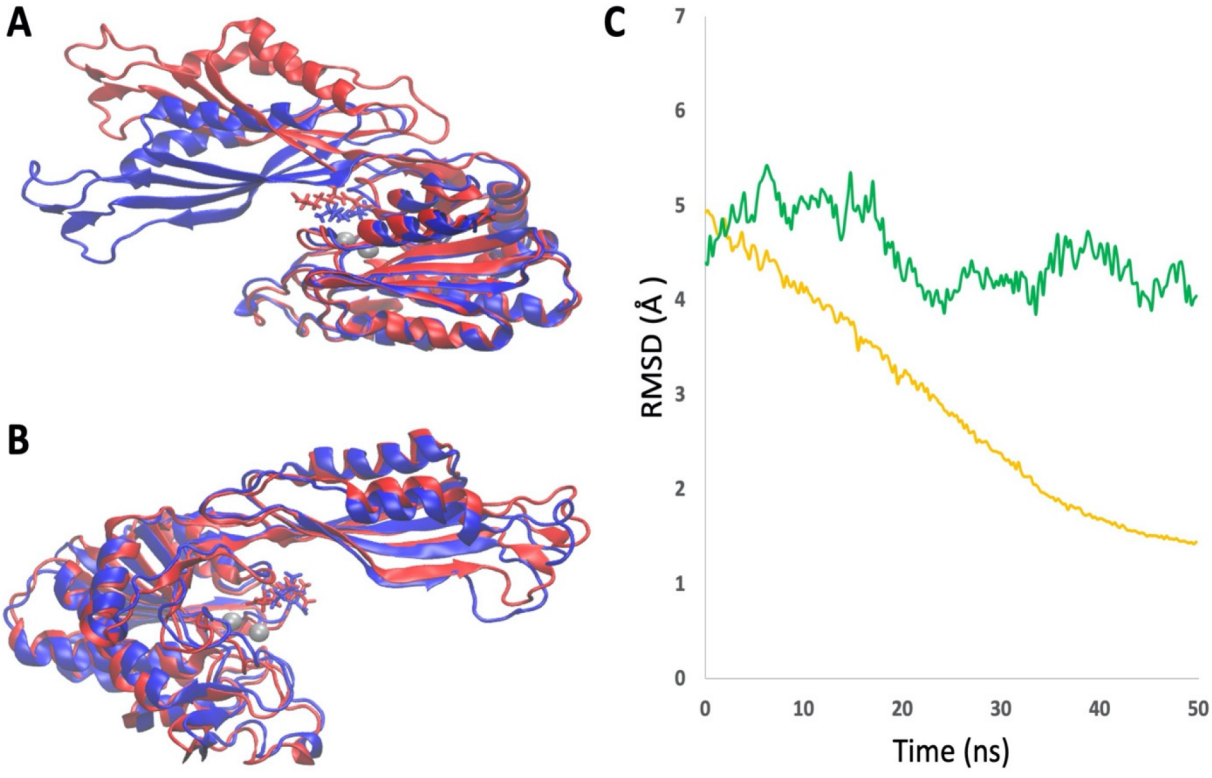

Figure 5. (A) Images of (A) subunit A and (B) subunit B of the DapE enzyme overlaid at 0 (red) and 50 ns (blue) in the simulation with the force only on subunit A. The substrate is also shown in both active sites in its position at 0 (red) and 50 ns (blue). (C) Average RMSDs between subunits A (orange) and B (green) in the open structure and their positions in the closed structure.

(PCA). They found that the first two principal components accounted for most of the essential dynamics of both structures but that the direction of protein movements depended on substrate binding. Although their study was done before the product-bound structure[12] was available, they were able to find a reasonable position for the substrate using molecular

https://dx.doi.org/10.1021/acs.biochem.0c00926
Biochemistry 2021, 60, 908−917

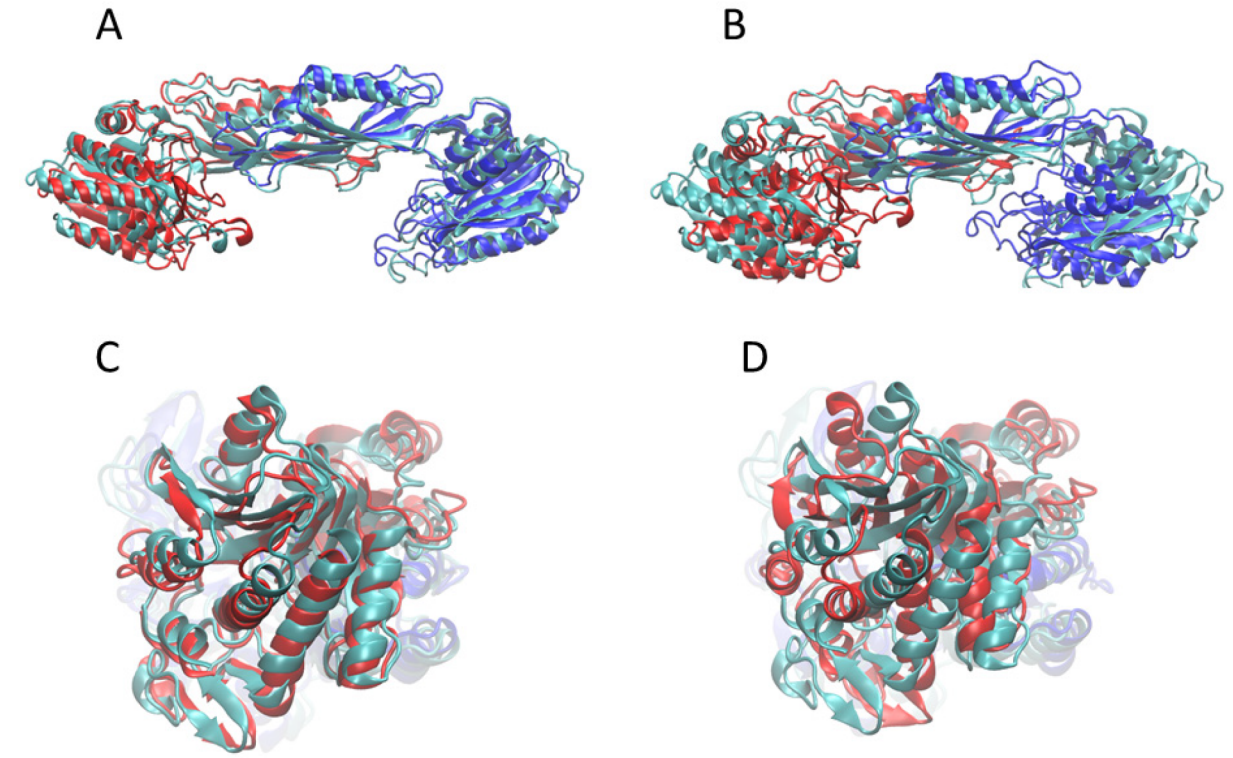

Figure 6. (A) DapE at 0 and 12.5 ns showing the conformational change in the catalytic domains moving toward the dimerization domains with force applied to both subunits. The dimer at time zero is colored cyan, and the dimer at 12.5 ns is colored red (chain A) and blue (chain B). (B) Same as panel A but at 40 ns. (C) Same as panel A but viewed so that the rotation of the catalytic domain relative to the dimerization domain can be seen easily. No rotation occurred during the first 12.5 ns of the TMD simulation. (D) Same as panel C but at 40 ns. The large rotation of the catalytic domain relative to the initial structure can be seen.

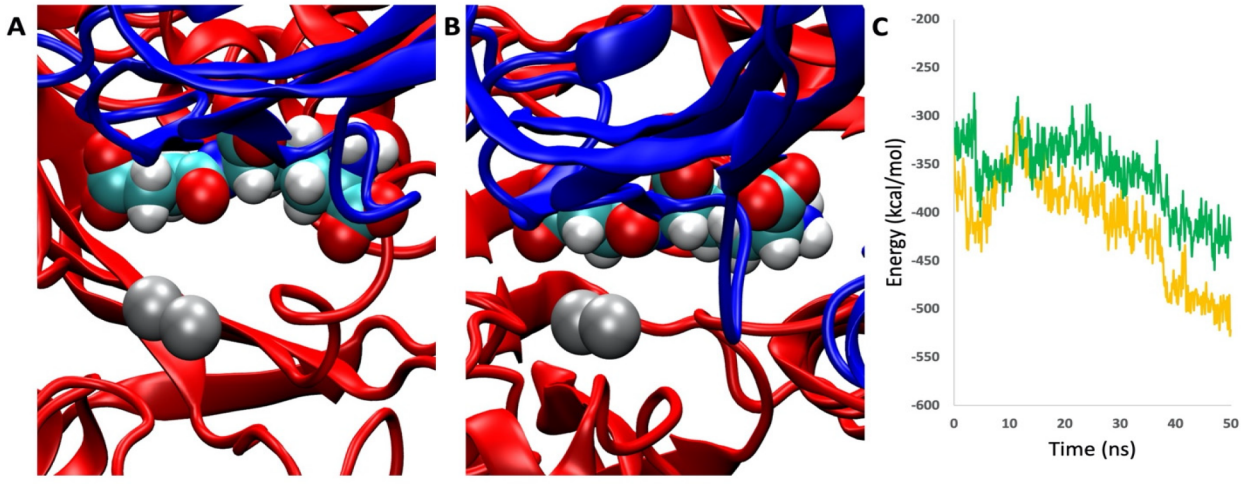

Figure 7. (A) Images of the active site of DapE at (A) 0 and (B) 50 ns with the substrate and the catalytic zinc atoms shown in the simulation with the force on both subunits. (C) Interaction energy between the substrate and the enzyme in subunit A (orange) and subunit B (green).

docking.[50] The first principal component of the L,L-SDAP-bound structure corresponded to the catalytic domains toward the dimerization domains, while the second was a rotation of the catalytic domains around the dimerization domains. Similar movements are seen in the TMD simulation presented here (Figure 6). There is a movement of the catalytic domains toward the dimerization domains during the first 12.5 ns of the simulation (Figure 6A) without a rotation of the catalytic domains relative to the dimerization domains (Figure 6C). By 40 ns into the simulation, the catalytic domains have completed their conformational changes (Figure 6B) due to a major rotation of the catalytic domains relative to the dimerization domains (Figure 6D).

Although no force was applied to the substrate, L,L-SDAP, it moved due to its interactions with the protein. As the subunits in the open conformation close, the substrate becomes further enveloped within the active site, and the distance between it and the catalytic zinc atoms decreases dramatically in both subunits in all three sets of simulations (Figure S6B1−3). The movement of the substrate is likely a result of the Coulombic

https://dx.doi.org/10.1021/acs.biochem.0c00926
Biochemistry 2021, 60, 908−917

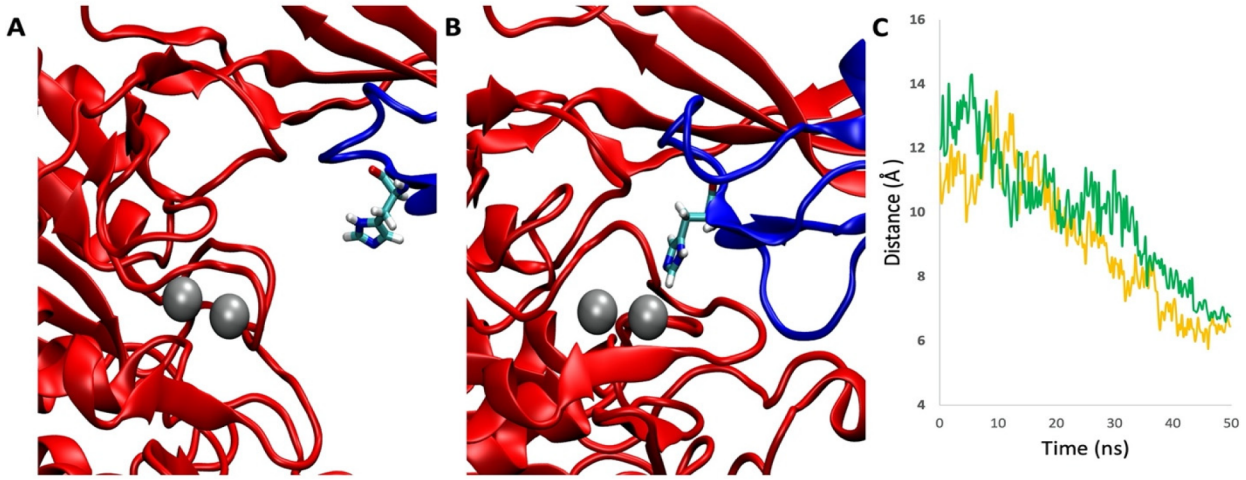

Figure 8. (A) Images of the active site of DapE at (A) 0 and (B) 50 ns with His195 and the catalytic zinc atoms shown in the simulation with the force on both subunits. (C) Distances from His195 to those zinc atoms in subunit A (orange) and subunit B (green).

attractions between two of the carboxyl groups in L,L-SDAP and Arg179 and Arg259 as well as a function of the movement of His195 from the communication domain of the opposite subunit. Arg179 interacts with the distal carboxylate group in the succinyl region of the substrate, while Arg259 interacts with the middle carboxylate group of the substrate (Figure S10). Upon observation of the initial and final positions of the substrate in all three sets of simulations, the substrate interacts consistently with both arginine residues, while at 50 ns, His195 has moved into the active site in the closed conformation, enabling its critical interaction with the substrate.

The Arg179 and Arg259 residues interact with the substrate initially (Figure 3B) and throughout the simulation (Figure S6D1−3,E1−3,G1−3), indicating that these arginine residues likely play a significant role in ferrying the substrate from its initial binding site further into the enzyme as it closes (Figure 7A,B). We had previously demonstrated inhibition of *Hi*DapE by addition of the arginine-specific chemical modification reagent 2,3-butanedione, indicating that at least one arginine residue interacts with the substrate.[12] His195B, by contrast, is much farther from the substrate but moves a significant distance (~6 Å) from the communication domain of the opposite subunit to participate in the active site and form the oxyanion hole that enables cleavage of the substrate.[12] His195B moves closer to the catalytic zinc atoms over the course of the conformational change and is in position to interact with the active site by the end of the simulation (Figure 8A−C and Figure S6C1−3). This motion should contribute to an overall stabilization as the substrate moves farther into the active site in the subunits that are closing. Calculated interaction energies between the substrate and the enzyme demonstrate that this is the case (Figure 6C). The substrate binds more tightly as the protein closes.

CONCLUSION

In summary, we have succeeded in crystallizing *Nm*DapE (PDB entry 5UEJ) in an open conformation structure with atomic-level resolution (1.3 Å). Comparison with other DapE structures demonstrates the flexibility of this protein. The new structure reveals two sulfates bound to active site Arg residues that have been implicated in substrate recognition and binding.[12] The presence of sulfate prompted us to determine the inhibitory potency of sulfate, which has an IC_{50} of 13.8 ± 2.8 mM. The sulfate positions suggested the binding site for the substrate in the open structure, so we employed this new structure as the starting point for TMD simulations studying the dramatic conformational change from the open to the closed conformation that occurs when DapE binds its substrate, L,L-SDAP. Addressing the possibility that the closure of the two subunits may be linked, these TMD studies reveal the independence of the two subunits. The TMD method enabled us to examine how different parts of the system might affect each other. By placing a force on only one of the subunits, we found that closing that subunit did not force the closure of the other subunit. Because the SDAP also did not have a force on it, the results showed how the substrate is pulled into position in the active site. Given our long-range goal of developing new antibiotics based on inhibitors of DapE, this is an important result. The conformational change of the protein results in the substrate moving toward the active site and increasing its binding affinity. These data provide new insight into the proposed catalytic mechanism as they confirm the ability of DapE to shift between an open conformation to a closed form upon the addition of the substrate. They further confirm that His195B can move >6 Å into the subunit A active site, a critical step in the catalytic process. The sulfates bound in the active site in the new high-resolution DapE crystal structure underscore the importance of the Coulombic interactions in binding the negatively charged carboxylates in the substrate. Understanding the energetics and geometry changes at play in closing DapE, revealed by TMD, informs the design of potential inhibitors that can lead to a closed or partially closed structure, which would be energetically favorable, versus inhibitors that bind to only the open conformer of DapE. These data provide an enhanced understanding of the key binding interactions in the active site of DapE that will enable the de novo design of inhibitors as well as optimization of existing lead structures.

ASSOCIATED CONTENT

Supporting Information

The Supporting Information is available free of charge at https://pubs.acs.org/doi/10.1021/acs.biochem.0c00926.

https://dx.doi.org/10.1021/acs.biochem.0c00926
Biochemistry 2021, 60, 908−917

X-ray collection and refinement statistics, analysis of DapE conformational changes, plots of inhibition by sulfate, and graphical analyses of targeted molecular dynamics (PDF)

Accession Codes

DapE, Uniprot entry Q9JYL2; Protein Data Bank entry 5UEJ.

AUTHOR INFORMATION

Corresponding Authors

Kenneth W. Olsen − *Department of Chemistry and Biochemistry, Loyola University Chicago, Chicago, Illinois 60660, United States;* orcid.org/0000-0001-7116-6321; Email: kolsen@luc.edu

Daniel P. Becker − *Department of Chemistry and Biochemistry, Loyola University Chicago, Chicago, Illinois 60660, United States;* orcid.org/0000-0001-9392-0460; Email: dbecke3@luc.edu

Authors

Matthew Kochert − *Department of Chemistry and Biochemistry, Loyola University Chicago, Chicago, Illinois 60660, United States;* orcid.org/0000-0003-1997-2128

Boguslaw P. Nocek − *The Center for Structural Genomics of Infectious Diseases, Computation Institute, The University of Chicago, Chicago, Illinois 60637, United States*

Thahani S. Habeeb Mohammad − *Department of Chemistry and Biochemistry, Loyola University Chicago, Chicago, Illinois 60660, United States;* orcid.org/0000-0002-5827-0922

Elliot Gild − *Department of Chemistry and Biochemistry, Loyola University Chicago, Chicago, Illinois 60660, United States*

Kaitlyn Lovato − *Department of Chemistry and Biochemistry, Loyola University Chicago, Chicago, Illinois 60660, United States*

Tahirah K. Heath − *Department of Chemistry and Biochemistry, Loyola University Chicago, Chicago, Illinois 60660, United States*

Richard C. Holz − *Department of Chemistry, Colorado School of Mines, Golden, Colorado 80401, United States;* orcid.org/0000-0001-6093-2799

Complete contact information is available at: https://pubs.acs.org/10.1021/acs.biochem.0c00926

Funding

This work was supported in part by the National Science Foundation (CHE-2003861, R.C.H.).

Notes

The authors declare no competing financial interest.

REFERENCES

(1) World Health Organization (2017) Antibacterial agents in clinical development: an analysis of the antibacterial clinical development pipeline, including tuberculosis.

(2) Klevens, R. M., Morrison, M. A., Nadle, J., Petit, S., Gershrnan, K., Ray, S., Harrison, L. H., Lynfield, R., Dumyati, G., Townes, J. M., Craig, A. S., Zell, E. R., Fosheim, G. E., Mcdougal, L. K., Carey, R. B., and Fridkin, S. K. (2007) Invasive methicillin-resistant staphylococcus aureus infections in the United States. *JAMA, J. Am. Med. Assoc. 298*, 1763−1771.

(3) Howe, R. A., Bowker, K. E., Walsh, T. R., Feest, T. G., and MacGowan, A. P. (1998) Vancomycin-resistant Staphylococcus aureus. *Lancet 351*, 602.

(4) Gillner, D. M., Becker, D. P., and Holz, R. C. (2013) Lysine biosynthesis in bacteria: a metallodesuccinylase as a potential antimicrobial target. *JBIC, J. Biol. Inorg. Chem. 18*, 155−163.

(5) Scapin, G., and Blanchard, J. S. (1998) Enzymology of bacterial lysine biosynthesis. *Adv. Enzymol. Relat. Areas Mol. Biol. 72*, 279−324.

(6) Heath, T. K., Lutz, M. R., Jr, Reidl, C. T., Guzman, E. R., Herbert, C. A., Nocek, B. P., Holz, R. C., Olsen, K. W., Ballicora, M. A., and Becker, D. P. (2018) Practical spectrophotometric assay for the dapE-encoded N-succinyl-L, L-diaminopimelic acid desuccinylase, a potential antibiotic target. *PLoS One 13*, No. e0196010.

(7) Karita, M., Etterbeek, M. L., Forsyth, M. H., Tummuru, M. K. R., and Blaser, M. J. (1997) Characterization of Helicobacter pylori dapE and construction of a conditionally lethal dapE mutant. *Infect. Immun. 65*, 4158−4164.

(8) Pavelka, M. S., Jr., and Jacobs, W. R., Jr (1996) Biosynthesis of diaminopimelate, the precursor of lysine and a component of peptidoglycan, is an essential function of Mycobacterium smegmatis. *J. Bacteriol. 178*, 6496−6507.

(9) Badger, J., Sauder, J., Adams, J., Antonysamy, S., Bain, K., Bergseid, M., Buchanan, S., Buchanan, M., Batiyenko, Y., Christopher, J., et al. (2005) Structural analysis of a set of proteins resulting from a bacterial genomics project. *Proteins: Struct., Funct., Genet. 60*, 787−796.

(10) Nocek, B. P., Gillner, D. M., Fan, Y., Holz, R. C., and Joachimiak, A. (2010) Structural Basis for Catalysis by the Mono- and Dimetalated Forms of the dapE-Encoded N-succinyl-L,L-Diaminopimelic Acid Desuccinylase. *J. Mol. Biol. 397*, 617−626.

(11) Starus, A., Nocek, B., Bennett, B., Larrabee, J. A., Shaw, D. L., Sae-Lee, W., Russo, M. T., Gillner, D. M., Makowska-Grzyska, M., Joachimiak, A., and Holz, R. C. (2015) Inhibition of the dapE-Encoded N-Succinyl-L,L-diaminopimelic Acid Desuccinylase from Neisseria meningitidis by L-Captopril. *Biochemistry 54*, 4834−4844.

(12) Nocek, B., Reidl, C., Starus, A., Heath, T., Bienvenue, D., Osipiuk, J., Jedrzejczak, R. P., Joachimiak, A., Becker, D. P., and Holz, R. C. (2018) Structural Evidence for a Major Conformational Change Triggered by Substrate Binding in DapE Enzymes: Impact on the Catalytic Mechanism. *Biochemistry 57*, 574.

(13) Reidl, C., Majorek, K. A., Dang, J., Tran, D., Jew, K., Law, M., Payne, Y., Minor, W., Becker, D. P., and Kuhn, M. L. (2017) Generating enzyme and radical-mediated bisubstrates as tools for investigating Gcn5-related N-acetyltransferases. *FEBS Lett. 591*, 2348−2361.

(14) Reidl, C. T., Heath, T. K., Darwish, I., Torrez, R. M., Moore, M., Gild, E., Nocek, B. P., Starus, A., Holz, R. C., and Becker, D. P. (2020) Indoline-6-Sulfonamide Inhibitors of the Bacterial Enzyme DapE. *Antibiotics 9*, 595.

(15) Dutta, D., and Mishra, S. (2018) L-Captopril and its derivatives as potential inhibitors of microbial enzyme DapE: A combined approach of drug repurposing and similarity screening. *J. Mol. Graphics Modell. 84*, 82−89.

(16) Mandal, R. S., and Das, S. (2015) In silico approach towards identification of potential inhibitors of Helicobacter pylori DapE. *J. Biomol. Struct. Dyn. 33*, 1460−1473.

(17) Rosenbaum, G., Alkire, R. W., Evans, G., Rotella, F. J., Lazarski, K., Zhang, R., Ginell, S. L., Duke, N., Naday, I., Lazarz, J., et al. (2006) The Structural Biology Center 19ID undulator beamline: facility specifications and protein crystallographic results. *J. Synchrotron Radiat. 13*, 30−45.

(18) Minor, W., Cymborowski, M., Otwinowski, Z., and Chruszcz, M. (2006) HKL-3000: the integration of data reduction and structure solutionâ€"from diffraction images to an initial model in minutes. *Acta Crystallogr., Sect. D: Biol. Crystallogr. 62*, 859.

(19) Vagin, A., and Teplyakov, A. (1997) MOLREP: an automated program for molecular replacement. *J. Appl. Crystallogr. 30*, 1022−1025.

(20) Emsley, P., Lohkamp, B., Scott, W. G., and Cowtan, K. (2010) Features and development of Coot. *Acta Crystallogr., Sect. D: Biol. Crystallogr. 66*, 486−501.

(21) Murshudov, G. N., SkubÃk, P., Lebedev, A. A., Pannu, N. S., Steiner, R. A., Nicholls, R. A., Winn, M. D., Long, F., and Vagin, A. A. (2011) REFMAC5 for the refinement of macromolecular crystal structures. *Acta Crystallogr., Sect. D: Biol. Crystallogr. 67*, 355.
(22) Davis, I. W., Leaver-Fay, A., Chen, V. B., Block, J. N., Kapral, G. J., Wang, X., Murray, L. W., Arendall, W. B., 3rd, Snoeyink, J., Richardson, J. S., and Richardson, D. C. (2007) MolProbity: all-atom contacts and structure validation for proteins and nucleic acids. *Nucleic Acids Res. 35*, W375−83.
(23) Emsley, P., and Cowtan, K. (2004) Coot: model-building tools for molecular graphics. *Acta Crystallogr., Sect. D: Biol. Crystallogr. D60*, 2126−2132.
(24) Humphrey, W., Dalke, A., and Schulten, K. (1996) VMD: visual molecular dynamics. *J. Mol. Graphics 14*, 33−8.
(25) Press, W. H., Flannery, B. P., Teukolsky, S. A., and Vetterling, W. T. (1988) *Numerical Recipes in C: The Art of Scientific Computing*, Cambridge University Press, New York.
(26) Figueroa, C. M., Esper, M. C., Bertolo, A., Demonte, A. M., Aleanzi, M., Iglesias, A. A., and Ballicora, M. A. (2011) Understanding the allosteric trigger for the fructose-1,6-bisphosphate regulation of the ADP-glucose pyrophosphorylase from Escherichia coli. *Biochimie 93*, 1816−1823.
(27) Altschul, S. F., Gish, W., Miller, W., Myers, E. W., and Lipman, D. J. (1990) Basic local alignment search tool. *J. Mol. Biol. 215*, 403−410.
(28) Sievers, F., Wilm, A., Dineen, D., Gibson, T. J., Karplus, K., Li, W., Lopez, R., McWilliam, H., Remmert, M., Soding, J., Thompson, J. D., and Higgins, D. G. (2011) Fast, scalable generation of high-quality protein multiple sequence alignments using Clustal Omega. *Mol. Syst. Biol. 7*, 539.
(29) Waterhouse, A., Bertoni, M., Bienert, S., Studer, G., Tauriello, G., Gumienny, R., Heer, F. T., de Beer, T. A. P., Rempfer, C., Bordoli, L., et al. (2018) SWISS-MODEL: homology modelling of protein structures and complexes. *Nucleic Acids Res. 46*, W296−W303.
(30) Waterman, M. S., and Eggert, M. (1987) A new algorithm for best subsequence alignments with application to tRNA-rRNA comparisons. *J. Mol. Biol. 197*, 723−728.
(31) Phillips, J. C., Braun, R., Wang, W., Gumbart, J., Tajkhorshid, E., Villa, E., Chipot, C., Skeel, R. D., Kale, L., and Schulten, K. (2005) Scalable molecular dynamics with NAMD. *J. Comput. Chem. 26*, 1781−1802.
(32) Vanommeslaeghe, K., Hatcher, E., Acharya, C., Kundu, S., Zhong, S., Shim, J., Darian, E., Guvench, O., Lopes, P., and Vorobyov, I. (2010) CHARMM general force field: A force field for drug-like molecules compatible with the CHARMM all-atom additive biological force fields. *J. Comput. Chem. 31*, 671−690.
(33) Best, R. B., Zhu, X., Shim, J., Lopes, P. E., Mittal, J., Feig, M., and MacKerell, A. D., Jr (2012) Optimization of the additive CHARMM all-atom protein force field targeting improved sampling of the backbone ϕ, ψ and side-chain χ1 and χ2 dihedral angles. *J. Chem. Theory Comput. 8*, 3257−3273.
(34) MacKerell, A. D., Jr, Feig, M., and Brooks, C. L. (2004) Improved treatment of the protein backbone in empirical force fields. *J. Am. Chem. Soc. 126*, 698−699.
(35) MacKerell, A. D., Jr, Bashford, D., Bellott, M., Dunbrack, R. L., Jr, Evanseck, J. D., Field, M. J., Fischer, S., Gao, J., Guo, H., Ha, S., et al. (1998) All-atom empirical potential for molecular modeling and dynamics studies of proteins. *J. Phys. Chem. B 102*, 3586−3616.
(36) Díaz-Sánchez, Ã G., Terrazas-López, M., Aguirre-Reyes, L. G., Lobo-Galo, N., Ã lvarez-Parrilla, E., and MartÃnez-MartÃnez, A. (2019) Aspectos estructurales y funcionales de la N-Succinil-L, L-diaminopimelato desuccinilasa, una enzima clave para el crecimiento bacteriano y un blanco para el control antimicrobiano. *TIP, Rev. Espec. Cienc. Quim.-Biol. 22*, n/a.
(37) Schiffer, M., Ainsworth, C., Xu, Z., Carperos, W., Olsen, K., Solomon, A., Stevens, F., and Chang, C. (1989) Structure of a second crystal form of Bence-Jones protein Loc: strikingly different domain associations in two crystal forms of a single protein. *Biochemistry 28*, 4066−4072.
(38) Eyal, E., Gerzon, S., Potapov, V., Edelman, M., and Sobolev, V. (2005) The limit of accuracy of protein modeling: influence of crystal packing on protein structure. *J. Mol. Biol. 351*, 431−442.
(39) Joshi, M., Gakhar, L., and Fuentes, E. J. (2013) High-resolution structure of the Tiam1 PHn-CC-Ex domain. *Acta Crystallogr., Sect. F: Struct. Biol. Commun. 69*, 744−752.
(40) Thompson, H. P., and Day, G. M. (2014) Which conformations make stable crystal structures? Mapping crystalline molecular geometries to the conformational energy landscape. *Chemical Science 5*, 3173−3182.
(41) Luo, J., Liu, Z., Guo, Y., and Li, M. (2015) A structural dissection of large protein-protein crystal packing contacts. *Sci. Rep. 5*, 14214.
(42) Ahmad, E., Rabbani, G., Zaidi, N., Khan, M. A., Qadeer, A., Ishtikhar, M., Singh, S., and Khan, R. H. (2013) Revisiting ligand-induced conformational changes in proteins: essence, advancements, implications and future challenges. *J. Biomol. Struct. Dyn. 31*, 630−648.
(43) Nocek, B., Starus, A., Makowska-Grzyska, M., Gutierrez, B., Sanchez, S., Jedrzejczak, R., Mack, J. C., Olsen, K. W., Joachimiak, A., and Holz, R. C. (2014) The dimerization domain in DapE enzymes is required for catalysis. *PLoS One 9*, e93593.
(44) Kanyo, Z. F., and Christianson, D. W. (1991) Biological recognition of phosphate and sulfate. *J. Biol. Chem. 266*, 4264−4268.
(45) Copley, R. R., and Barton, G. J. (1994) A Structural Analysis of Phosphate and Sulphate Binding Sites in Proteins: Estimation of Propensities for Binding and Conservation of Phosphate Binding Sites. *J. Mol. Biol. 242*, 321−329.
(46) Moras, D., Olsen, K. W., Sabesan, M. N., Buehner, M., Ford, G. C., and Rossmann, M. G. (1975) Studies of asymmetry in the three-dimensional structure of lobster D-glyceraldehyde-3-phosphate dehydrogenase. *J. Biol. Chem. 250*, 9137−9162.
(47) Dutta, D., and Mishra, S. (2016) Structural and mechanistic insight into substrate binding from the conformational dynamics in apo and substrate-bound DapE enzyme. *Phys. Chem. Chem. Phys. 18*, 1671−1680.
(48) Weng, J., Fan, K., and Wang, W. (2012) The conformational transition pathways of ATP-binding cassette transporter BtuCD revealed by targeted molecular dynamics simulation. *PLoS One 7*, e30465.
(49) Cheng, X., Wang, H., Grant, B., Sine, S. M., and McCammon, J. A. (2006) Targeted molecular dynamics study of C-loop closure and channel gating in nicotinic receptors. *PLoS Comput. Biol. 2*, e134.
(50) Dutta, D., and Mishra, S. (2014) The structural and energetic aspects of substrate binding and the mechanism of action of the DapE-encoded N-succinyl-L,L-diaminopimelic acid desuccinylase (DapE) investigated using a hybrid QM/MM method. *Phys. Chem. Chem. Phys. 16*, 26348−26358.

https://dx.doi.org/10.1021/acs.biochem.0c00926
Biochemistry 2021, 60, 908−917